

Effect of high-or low-speed fluctuations on the small-scale bursting events in an active control experiment

Xiao-Tong Cui(崔晓通), Nan Jiang(姜楠), and Zhan-Qi Tang(唐湛棋)
Citation: Chin. Phys. B, 2021, 30 (**1**): 014702. DOI: 10.1088/1674-1056/abc7a9
Journal homepage: http://cpb.iphy.ac.cn; http://iopscience.iop.org/cpb

What follows is a list of articles you may be interested in

Coherent structures over riblets in turbulent boundary layer studied by combining time-resolved particle image velocimetry (TRPIV), proper orthogonal decomposition (POD), and finite-time Lyapunov exponent (FTLE)

Shan Li(李山), Nan Jiang(姜楠), Shaoqiong Yang(杨绍琼), Yongxiang Huang(黄永祥), Yanhua Wu(吴彦华)
Chin. Phys. B, 2018, 27 (**10**): 104701. DOI: 10.1088/1674-1056/27/10/104701

Active control of wall-bounded turbulence for drag reduction with piezoelectric oscillators

Jian-Xia Bai(白建侠), Nan Jiang(姜楠), Xiao-Bo Zheng(郑小波), Zhan-Qi Tang(唐湛琪), Kang-Jun Wang(王康俊), Xiao-Tong Cui(崔晓通)
Chin. Phys. B, 2018, 27 (**7**): 074701. DOI: 10.1088/1674-1056/27/7/074701

Particle transport behavior in air channel flow with multi-group Lagrangian tracking

Hao Lu(卢浩), Wen-Jun Zhao(赵文君), Hui-Qiang Zhang(张会强), Bing Wang(王兵), Xi-Lin Wang(王希麟)
Chin. Phys. B, 2017, 26 (**1**): 014702. DOI: 10.1088/1674-1056/26/1/014702

Predetermined control of turbulent boundary layer with a piezoelectric oscillator

Xiao-Bo Zheng(郑小波), Nan Jiang(姜楠), Hao Zhang(张浩)
Chin. Phys. B, 2016, 25 (**1**): 014703. DOI: 10.1088/1674-1056/25/1/014703

Experimental study on spectrum and multi-scale nature of wall pressure and velocity in turbulent boundary layer

Zheng Xiao-Bo, Jiang Nan
Chin. Phys. B, 2015, 24 (**6**): 064702. DOI: 10.1088/1674-1056/24/6/064702

Effect of high- or low-speed fluctuations on the small-scale bursting events in an active control experiment*

Xiao-Tong Cui(崔晓通)[1], Nan Jiang(姜楠)[1,2,†], and Zhan-Qi Tang(唐湛棋)[1,2,‡]

[1] *Department of Mechanics, Tianjin University, Tianjin* 300354, *China*
[2] *Tianjin Key Laboratory of Modern Engineering Mechanics, Tianjin* 300354, *China*

(Received 24 September 2020; revised manuscript received 15 October 2020; accepted manuscript online 5 November 2020)

Active control of a fully developed turbulence boundary layer (TBL) over a flat plate has been investigated with a statistical view. The piezoelectric (PZT) oscillator is employed to produce periodic input into the inner region of the TBL. A wall probe is fixed upstream of the oscillator to identify the high- or low-speed fluctuations as the detecting signals. Then, the impact of the detecting signals on the small-scale bursting process is investigated based on the data acquired by the traversing probe downstream of the oscillator. The results indicate that the small-scale bursting intensity is restrained more apparently at high-speed detecting fluctuations but less impacted at low-speed detecting fluctuations. Furthermore, the perturbed-scale fluctuations arrange the small-scale bursting process in the near-wall region. The detecting signals have an obvious impact on this arrangement, especially the high-intensity regions of the small-scale bursting events: the vibration enhances the intensity at high-speed detecting signals but weakens it at low-speed detecting signals in these regions, which gives a direct evidence on how detecting signals interfering the small-scale bursting process.

Keywords: turbulent boundary layer, active control, discrete wavelet decomposition, small-scale bursting process

PACS: 47.85.lb, 47.85.ld, 47.27.nb, 47.27.De **DOI:** 10.1088/1674-1056/abc7a9

1. Introduction

Over the past few decades, there has been growing understanding that turbulent boundary layers (TBL), in spite of their apparent randomness, possess certain recurrent features, which are usually defined as "coherent structures".[1,2] These motions transport momentum in TBL and provide a means of producing turbulent kinetic energy.[3,4] Moreover, the coherent structures such as streamwise vortices and velocity streaks (which constitute the near-wall cycle) also play a key role in turbulent flow control.[5–8] The bursting events of the near-wall cycle are closely related to the skin friction distribution.[9] Thus, it is meaningful to extract and evaluate these structures in flow control studies.[10–12] There are serval detecting methods on coherent structures. Blackwelder and Kaplan first explored the variable integration time averaging technique (VITA).[1] By this technique, an event is assumed to occur when the short time variance exceeds a certain threshold multiple of the mean square signal.[13] The *u*-level or *mu*-level method also has been applied in numerous studies.[14,15] Combining the coherent structures and intermittency, Camusi *et al.*[16,17] introduced another way to detect these structures based on the wavelet transform in homogeneous and isotropic turbulence. Here, intermittency is related to the non-Gaussian distribution of the velocity gradients or the rate of turbulent energy dissipation. After that, this method was also applied in inhomogeneous and anisotropic flow conditions.[6,18–20]

As mentioned above, quasi streamwise vortices (QSV) are the typical coherent structures, which contain ejection and sweep processes.[21–24] The ejection process occurs on the updraft side of QSVs, wherein the low-speed fluids in the inner layer are lifted away from the wall to the outer layer. The sweep process occurs on the downdraft side of QSVs, wherein the high-speed fluids move downward to the wall. Because of the close relationship with skin friction,[25,26] these processes often were selectively controlled in numerous drag reduction DNS or experimental studies. Carlson and Lumley[27] employed a Gaussian bump as an actuator for opposition control. While the sweep events were detected, the bump would be activated to push the high-speed fluctuations away from the wall. Xu *et al.*[11] also studied the active control of the near-wall streamwise vortices via DNS databases of fully developed turbulent channel flow at a low Reynolds number. Choi *et al.*[9] conducted the experimental research by using the opposition control to suppress the downwash of high-speed fluid during the sweep events to reduce the skin-friction drag. In their research, a hot-wire probe was fixed on the test surface to detect the sweep events by measuring the temporal change of streamwise fluctuations in the near-wall region of TBL.

Nevertheless, relatively less attention was paid to how the high- or low-speed detecting signals affect the response of near-wall bursting events to the control, which could help us to develop a potential approach to modify the turbulence

*Project supported by the National Natural Science Foundation of China (Grant Nos. 11972251, 11732010, 11572221, 11502066, and 11872272).
†Corresponding author. E-mail: nanj@tju.edu.cn
‡Corresponding author. E-mail: zhanqitang@tju.edu.cn
© 2021 Chinese Physical Society and IOP Publishing Ltd

boundary layer flows. In this paper, a further step is taken on the basis of Tang *et al.*'s study.[6] A piezoelectric (PZT) vibrator was employed to produce periodic synthetic input into the near-wall region of TBL and the TBL hot-wire probe was settled downstream of the vibrator to measure the u-component velocity at various locations in TBL. By setting a single-filament hot-wire probe in front of the actuator as the detector, we could identify the high or low fluctuations and then investigate the impact of the detecting signals on the bursting events. It should be noted that the high or low speed fluctuations mean the positive or negative value of detecting signals in this paper. Furthermore, because the small-scale intermittent events were correlated with highly spatial-temporal coherent structures,[16,28] we would focus on the impact on the small-scale bursting events in this research. The paper is organized as follows. The experimental setup is introduced in Section 2. In Subsection 3.1, the drag reduction results and other basic parameters are summarized. The methodologies used for detecting signals (high or low speed fluctuations) and the small-scale intermittent events are described in Subsections 3.2 and 3.3. In Subsection 3.4, the impact of the detecting signals on the small-scale bursting events is analyzed. Finally, conclusions are listed in Section 4.

2. Experimental setup and conditions

The experiments were conducted in a closed loop wind tunnel in Tianjin University. Figure 1 shows the sketch of the experimental setup. The coordinates x, y, and z refer to the streamwise, wall normal, and spanwise directions, respectively. TBL flow developed along a flat plate, which was mounted vertically in the test section. The pitch angle was adjusted to assure a zero-pressure gradient in the streamwise direction. A tripwire was fixed at $x = 80$ mm downstream of the leading edge, and a sandpaper band was attached following the tripwire to accelerate the flow transition.

The freestream velocity was $U_\infty = 9$ m/s. TBL was fully developed before the control mechanism and the positions of measurement, which were located after $x = 1200$ mm. The Reynolds number was $Re_\tau = \delta u_\tau / \nu = 560$, where δ is the boundary layer thickness, u_τ is the friction velocity, and ν is the kinematic viscosity.

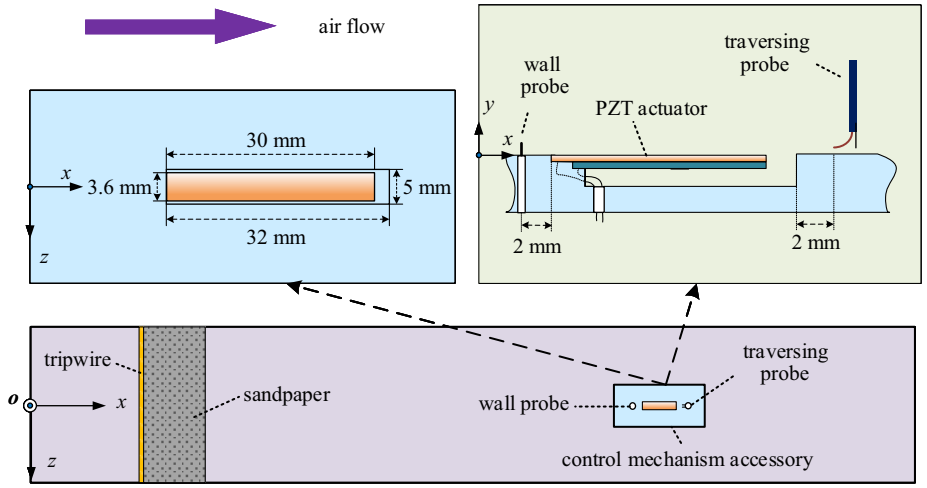


Fig. 1. Schematic of the experimental setup.

The control mechanism consisted a PZT element, which was flush-mounted with the plate surface (see Fig. 1). It has a dimension of 30 mm × 0.42 mm × 3.62 mm (length × thickness × width). In order to achieve better control effect, the PZT actuated frequency (f_p) was set at 160 Hz, which corresponds to the vortex shedding frequency in the near-wall region.[29,30] The amplitudes of actuator's free end were $A_p = 0.6$ mm, 0.4 mm, 0.1 mm corresponding to the driving voltages of $U_p = 80$ V, 50 V, 20 V, respectively.

Two hot-wire probes were used in the present study, both of which were operated by the TSI IFA-300 hot-wire anemometer unit in constant temperature mode. The calibration of these two probes was conducted using an air velocity calibrator over the velocity range 0–15 m/s. The first probe was used to measure the u-component velocity at various locations in TBL, thus referred to as the traversing probe. It is a TSI-1621 A-T1.5 miniature boundary layer probe. The sensing element of the probe is a tungsten wire with a diameter of 4 μm and a length of 1.25 mm. The probe was mounted on a 200 mm-long right-angle support, which was attached to a three-dimensional traverse gear. The traversing resolution was 5 μm in all directions. The traversing probe was used to map the u-component velocity at 62 different normal locations. The second hot-wire probe was a wall-mounted sensor to detect the bursting events by measuring the temporal change of the u-component velocity in the near-wall region of the TBL, which was referred to as the wall probe (see Fig. 1). This is a TSI straight probe, made of a tungsten wire of 4 μm in diameter

and 1.25 mm long. The wall probe was fixed on an adjustable bracket behind the flat plate, and stretched out through a small hole on the plate (see Fig. 1). The sensing wire was positioned on the required height ($y^+ = 14$ in the current study). Melted wax was then poured into the hole and the surface was made flush with the surrounding test-plate surface after the wax was cured. This construction of the wall probe allowed only the sensing wire and prong tips exposed to the flow without causing aerodynamic interference with the probe body. During the experiments, these two probes acquired data simultaneously, which mean they both obtained 62 different time sequences in each case. The sampling rate and low pass cut-off frequency were 100 and 50 kHz, respectively. Each sequence comprised of 2^{22} velocity samples or approximately 42 s.[31]

3. Results and discussion

3.1. Basic flow structures

Figure 2 shows the distribution of mean velocity in inner scaling, $U^+ = U/u_\tau$, where u_τ is the friction velocity. The mean velocity, U^+, is a function of wall-normal positions, $y^+ = yu_\tau/\nu$. Based on the data in the viscous sublayer, u_τ could obtained by[32–34]

$$\tau_w = \rho \nu \partial U/\partial y, \tag{1}$$

$$u_\tau = \sqrt{\bar{\tau}_w/\rho}, \tag{2}$$

where the air flow density is 1.205 kg/m^3 and the kinematic viscosity coefficient ν is 1.5×10^{-5} m^2/s. The overbar denotes time averaging. The local skin-friction reduction is defined as follows:

$$R_f = \frac{(\bar{\tau}_w)_{\text{on}} - (\bar{\tau}_w)_{\text{off}}}{(\bar{\tau}_w)_{\text{off}}} \times 100\%, \tag{3}$$

where the subscripts on and off denote measurements with and without control, respectively. The reduction rate and other fundamental parameters are presented in Table 1. It can be seen that case C acquires the lowest reduction rate of $R_f = 4\%$, and case A obtains the highest value of $R_f = 18\%$. The results confirm that with f_p kept constant, the drag reduction effect is positively correlated with A_p.[21,23]

As shown in Fig. 2, the velocity curve of the uncontrolled case fits well with linear law and log law, indicating a full developed TBL in the measuring location. As for different controlled cases, there are varying degrees of up-shifts in the logarithmic region. As indicated by other researches,[35,36] this change is the visual evidence of control effect in the view of whole TBL and the results also agree well with the reduction rates in Table 1.

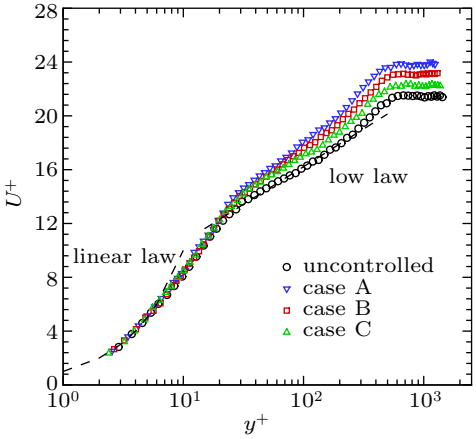


Fig. 2. Distributions of the mean streamwise velocity in the inner scaled units.

Table 1. Summary of the experimental parameters.

Case	U_∞ (m/s)	Re_τ	δ (m)	l/d	u_τ (m/s)	f_p (Hz)	A_p (mm)	R_f (%)
Uncontrolled	9.0	560	0.02	312	0.42	0	0	0
A	9.0	453	0.02	312	0.35	160	0.5	−18.0
B	9.0	506	0.02	312	0.38	160	0.3	−9.5
C	9.0	533	0.02	312	0.40	160	0.2	−4.7

3.2. Wavelet transforms

The wavelet transform is employed to investigate the impact of high or low fluctuations (the wall probe's data) on the multiscale bursting properties (the traversing probe's data). As a natural tool for relating anomalous scaling, intermittency, and bursting processes, the wavelet transform is introduced in many previous works such as Farge[37] and Daubechies.[38] So, a brief description is presented in this paper. The discrete orthonormal wavelet transform (DWT) was used in our research because of its advantage on the computing efficiency and avoiding redundant information. By the DWT, the fluctuation signals $u(t)$ can be decomposed into a series of self-similar orthonormal functions obtained via dilatations and translations of a mother wavelet $\psi\left(\frac{t-t'}{r}\right)$. The wavelet coefficients could be obtained as follows:

$$w(r,t') = \frac{1}{\sqrt{r}} \int_{-\infty}^{\infty} \psi^* \left(\frac{t-t'}{r}\right) u(t)\,\mathrm{d}t, \tag{4}$$

where r and t' are the wavelet scale and time, and the superscript * refers to the complex conjugate. The convolution is calculated in the frequency domain in each scale, thus $u(t)$ is decomposed in scale-time space. The Daubechies wavelet (db$N$, $N = 4$, N is the number of vanishing moments) is employed in this work, which is compactly supported orthonormal. By db4 wavelet, each time sequence of the velocity fluc-

tuation could be decomposed into 19 different scales in our study.

Then, we make some definitions for clarity. Based on the previous study,[6,21] the PZT perturbed frequency $f_p = 160$ Hz is between the characteristic frequencies of scales $r = 8$ and $r = 9$. Thus, the perturbed-scale mode is estimated by $u_P = w(8) + w(9)$, which represents the periodical forcing input by the actuator. Correspondingly, the wavelet scales $r < 8$ are defined as small scales, and the scales $r > 9$ are defined as large scales. Based on the definition, the small- and large-scale modes could be extracted as $u_S = \sum_{i=1}^{i=7} w(i)$ and $u_L = \sum_{i=10}^{i=19} w(i)$, respectively. Figure 3 shows the representative distribution of the fluctuation velocity $u(t)$ at the wall-normal height of $y^+ = 13$ in case A and its wavelet coefficients in different modes (u_S, u_L, and u_P).

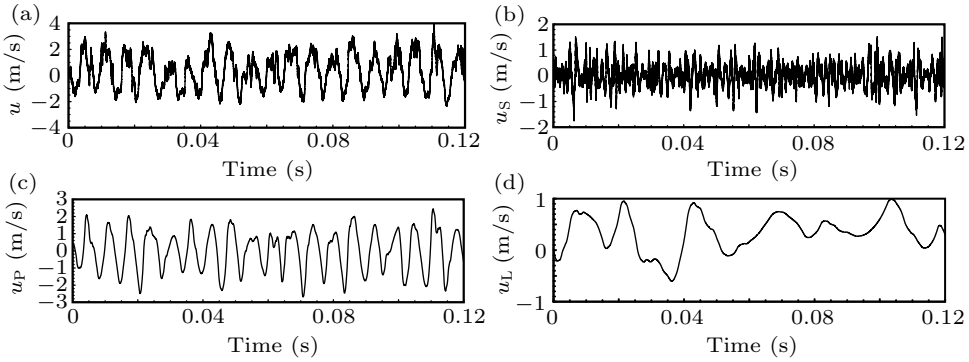


Fig. 3. Example of raw fluctuation signals [$u(t)$] at a wall normal position of $y^+ = 14$ in case A and the wavelet coefficients in different modes (small-scale mode [$u_S(t)$], perturbed mode [$u_P(t)$], and large-scale mode [$u_L(t)$]).

3.3. Methods for events detection

As mentioned above, a wall probe was fixed upstream of the vibrator to detect the high- and low-fluctuations at $y^+ = 14$, which could reflect the characteristics of the near-wall coherent structures.[9,30] According to Kreplin and Eckelmann,[39] the coherent structures could be observed over a streamwise distance $\Delta x^+ > 1000$. The study reported by Johansson *et al.*[40] also indicated that these structures are prevalent and persistent features of the near-wall region. In this work, the distance between the wall probe and the free end of the vibrator is $\Delta x_1^+ = 896$, which must be larger than the actuator length and also ensure that most of passing coherent structures' major characteristics are largely unchanged. The traversing probe is 4 mm ($\Delta x_2^+ = 112$) downstream of the free end of the vibrator, which guarantees that the probe could effectively catch the perturbation effect of the oscillator on the coherent structures. Moreover, the large-scale components are more robust than the small-scale fluctuations in TBL, so we extracted the large-scale signals to detect the high- and low-fluctuations. It would ensure as much relevance between the fluctuation signals of the wall probe and traversing probe as possible.

Figure 4 shows the maximum correlation coefficient (r_{max}) of the large-scale fluctuating components between the wall probe and the traversing probe. It can be obtained as follows:

$$r_{u_L u_{dL}}(\tau) = \frac{\overline{u_L(t) u_{dL}(t \pm \tau)}}{u_{L,RMS} u_{dL,RMS}}, \tag{5}$$

where u_L and u_{dL} are the large-scale fluctuating components of output signals from the traversing probe and the wall probe, respectively, and subscript 'RMS' represents their RMS values. The τ_c corresponds to the maximum $r_{u_L,u_{dL}}$, as illustrated in Fig. 4. Based on the result of τ_c, the convection velocity could be calculated, which remains nearly constant at $u^+ \approx 11$ in the near wall region ($y^+ < 27$). This compares well with the results of Kreplin and Eckelman,[39] who observed that coherent structures convect at a speed of $u^+ \approx 12$. Johansson *et al.*[40] found the convection velocity to be almost constant in the near-wall region of the turbulent boundary layer up to $y^+ = 30$. Furthermore, based on the former study by Tang and Zheng,[30,41] the impact of the vibrator concentrates mainly on $y^+ < 100$, and as shown in Fig. 4, the peak values of $r_{u_L,u_{dL}}$ are relatively large ($r_{max} > 0.3$) in this region ($y^+ < 100$). So, we would focus on the near-wall region in the following multi-scale intermittent bursting events study.

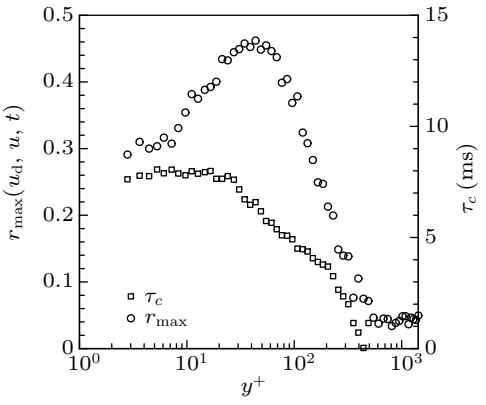


Fig. 4. The circles represent the peak cross-correlation values after allowing suitable time shift between the u-component velocities measured by the wall probe (at $y^+ = 14$) and the traversing probe in the downstream. The rectangles show the time shift applied to obtain peak cross-correlation values.

About the local intermittent bursting event analysis, two principal indicators are employed to extract the bursting signals in current study, which have been confirmed by former works.[6,16,21]

Flatness factor is defined as follows:[42]

$$FF(r) = \frac{\langle w(r,t)^4 \rangle}{\langle w(r,t)^2 \rangle^2}. \tag{6}$$

This function gives the level of intermittency at the scale. So, the difference with respect to the Gaussian statistics with $FF(r) = 3$ could be directly assessed.

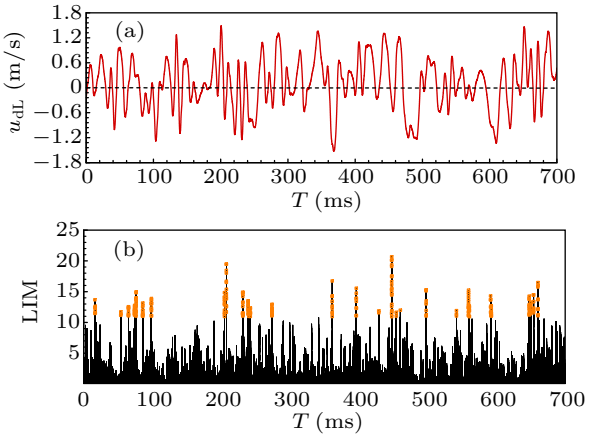


Fig. 5. (a) The large-scale fluctuating signals u_{dL}. (b) Example of LIM(r,t) (black line) and the detected small-scale bursting event (orange squares).

Local intermittency measure (LIM) is defined as follows:[37]

$$\mathrm{LIM}(r,t) = \frac{w(r,t)^2}{\langle w(r,t)^2 \rangle}. \tag{7}$$

The quantity $w(r,t)^2$ in this function might be interpreted as the energy contained in the fluctuating signals at scale r. Thus the LIM could enhance non-uniform distributions of energy, which is a good qualitative indicator of intermittency and of the magnitude of the energy fluctuations.[16] Following the study of Tang *et al.*,[5] we could localize the coherent structures for all scales by these two indicators. Figure 5(b) shows the intermittent energy bursting segments LIM (black line) and the intermittent bursting segments (orange symbols) selected using the above method at small scale (u_S) at $y^+ = 13$ in case A. As can be seen, the high peaks (orange symbols) reflect the existence of coherent structures, which should correspond to a high energy level. Moreover, these structures also show the distinct intermittency, which are not space filling in the temporal domain. Figure 5(a) shows the large-scale fluctuating signals u_{dL} obtained by the wall probe at the same time sequence with the LIM in Fig. 5(b). It seems that most of the small-scale bursting events are coupled with the appearance of the positive fluctuation of u_{dL}. Tang *et al.*[6] indicated that there was a clear correlation between the positive velocity of the perturbed-scale mode u_P and the small-scale bursting events. In this work, we take a further exploration on how detecting signals u_{dL} interfere the relationship between u_P and the small-scale bursting events.

3.4. The effect of the large-scale detecting signals on small-scale bursting event

Based on the discussion above, we believe that the LIM(r,t) is not only a measure of turbulent intermittency, but also an indicator of the energy burst magnitude. Therefore, the coherent structure signals at the specific scale of r could be extracted as follows:

$$w_b(r,t) = \begin{cases} w(r,t), & \mathrm{LIM}(r,t) > \mathrm{th}(r), \\ 0, & \mathrm{LIM}(r,t) \leqslant \mathrm{th}(r). \end{cases} \tag{8}$$

As an example, the orange symbols in Fig. 6 represent the small-scale bursting signals selected by formula (8) at $y^+ = 13$ in case A. Additionally, for observing the small-scale intermittent events from the statistical view more comprehensively, we define T_b as the time between the leading edges of successive bursting periods, ΔT as the time between the trailing and leading edges of a single bursting period.[15] The bursting frequency ($f_b = 1/\langle T_b \rangle$) is calculated based on the mean bursting period.[14]

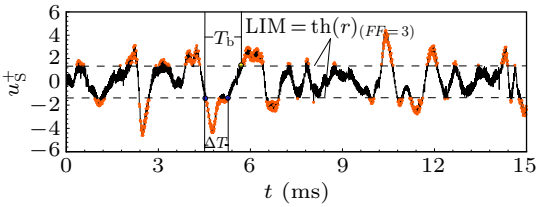


Fig. 6. Example of the bursting events (orange dots) detected from the small-scale fluctuations (black line). The time between successive events is denoted by T_b; while the duration of the event is denoted by ΔT.

The root mean square (rms) value of velocity fluctuations could reflect the mean turbulence energy intensity. Therefore, as shown in Figs. 7(a)–7(c), the ratios of $u_{brms,S}$ and $u_{rms,S}$ in different cases are calculated to describe the relative importance of the bursting process.[21] Here, $u_{brms,S}$ represents the mean rms values of the small-scale bursting signals, and $u_{rms,S}$ represents the mean rms values of the small-scale fluctuations. As can be seen, the perturbation apparently weakens the small-scale bursting process in the near-wall region (about $y^+ < 30$) in all controlled cases, and case A has the best performance. Previous studies have confirmed that the disturbance could diminished the bursting intensity of the original fluctuations, which is considered to be associated with the weakening of streamwise vortices in the buffer layer.[9,23] Figure 7 further indicates that the small-scale components of bursting events are similarly interfered by the vibration. Besides, in each controlled case, the detecting signals u_{dL} have a clear impact on the small-scale bursting process: while $u_{dL} < 0$, the value of $u_{brms,S}/u_{rms,S}$ (blue line) is lower than the no-detection controlled condition (red line) in the near-wall region. This variation may indicate that the perturbation decreases the bursting

intensity more efficiently at low-speed detecting signals. On the contrary, when $u_{\mathrm{dL}} > 0$, the value of $u_{\mathrm{brms,S}}/u_{\mathrm{rms,S}}$ (green line) gets higher than the no-detection controlled condition, which indicates a growth in bursting intensity.

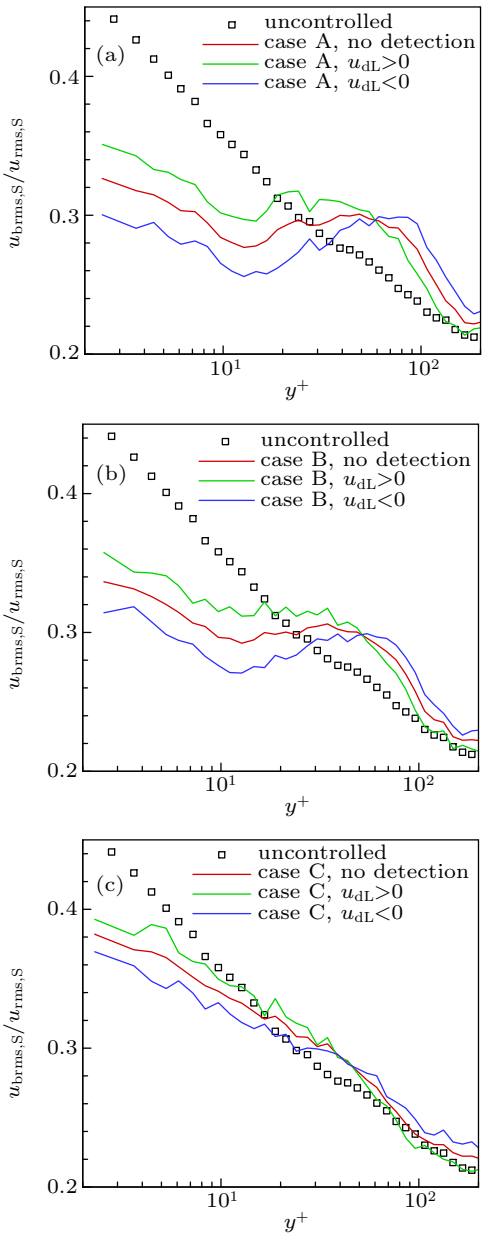


Fig. 7. The ratios of the rms value of the small-scale bursting signals ($u_{\mathrm{brms,S}}$) and the small-scale fluctuations ($u_{\mathrm{rms,S}}$).

Figure 8 presents the non-dimensional small-scale bursting frequency (f_{bS}^+) in all cases. As can be seen, by the vibration, the bursting frequencies are significantly lower than the f_{bS}^+ in the uncontrolled case. It reflects that the formation of the small-scale bursting process is suppressed by the perturbation in the near-wall region, which is consistent with the finding in Fig. 7. Moreover, in the near-wall region, it seems that the vibration restrains the bursting events more effectively than the no-detection condition at $u_{\mathrm{dL}} < 0$, but has the opposite effect when $u_{\mathrm{dL}} > 0$. In Figs. 7 and 8, it also should be noted that the impact of the detecting signals on the bursting process is positive correlated with amplitude A_{p}.

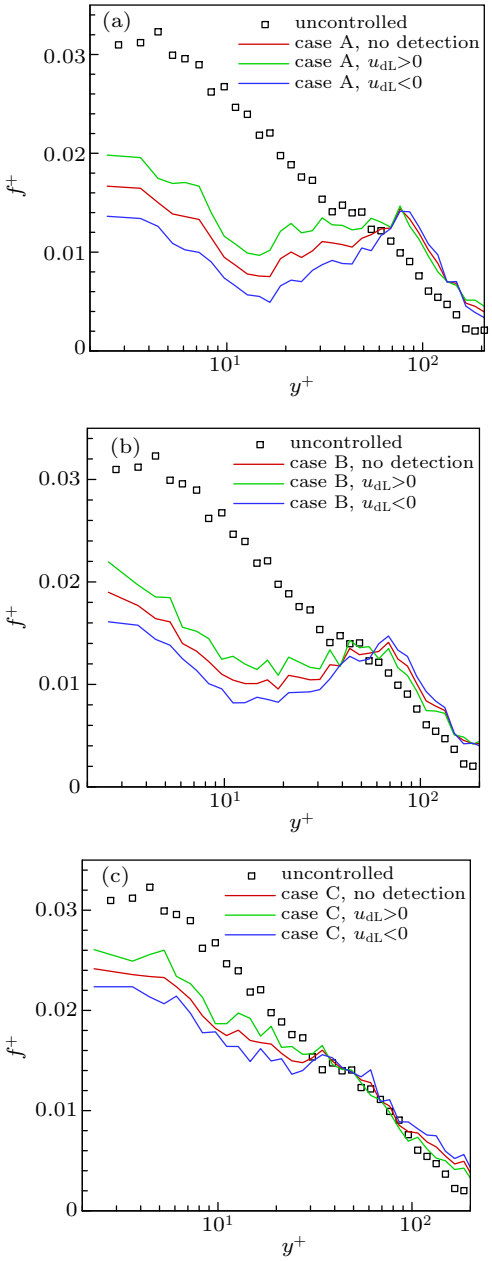


Fig. 8. The distribution of bursting frequency ($f_{\mathrm{b}} = 1/\langle w_{\mathrm{b}}(r,t)^2\rangle$) in different cases.

Figure 9 gives the distribution of the non-dimensional small-scale bursting duration ΔT_{bS}^+ in different cases. It is shown that the bursting duration is shortened by controlling in the near-wall region, but not sensitive to the detecting signals in all controlled cases. In general, according to the statistical results, we confirm that the small-scale bursting events could be weakened by the oscillation, and the performance is dependent on the PZT oscillating amplitude. More interestingly, from the statistical view, the detecting signals u_{dL} clearly affected the control, which might indicate that the vibration could suppress the small-scale bursting process more effectively at low-speed fluctuations ($u_{\mathrm{dL}} < 0$), but have less impact at high-speed fluctuations ($u_{\mathrm{dL}} > 0$).

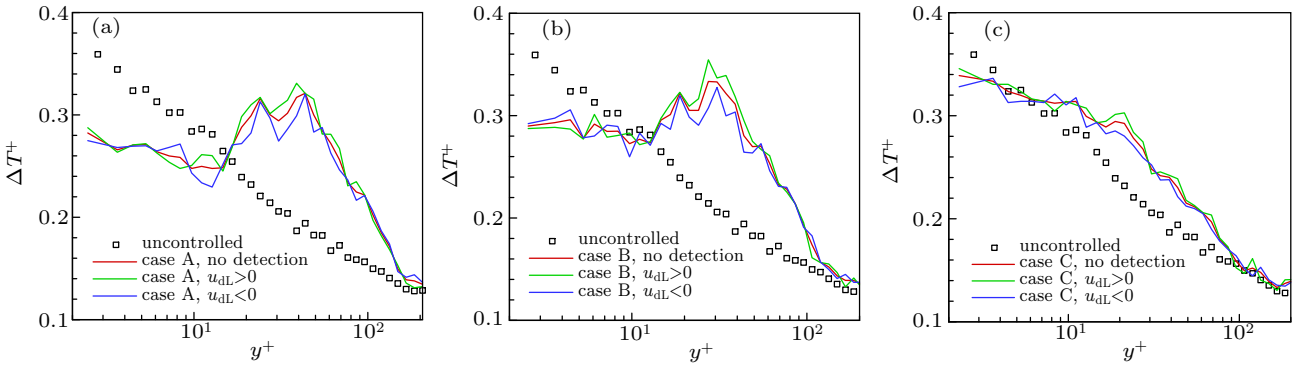


Fig. 9. The distribution of the duration of the bursting event ($\langle \Delta T \rangle$) in different cases.

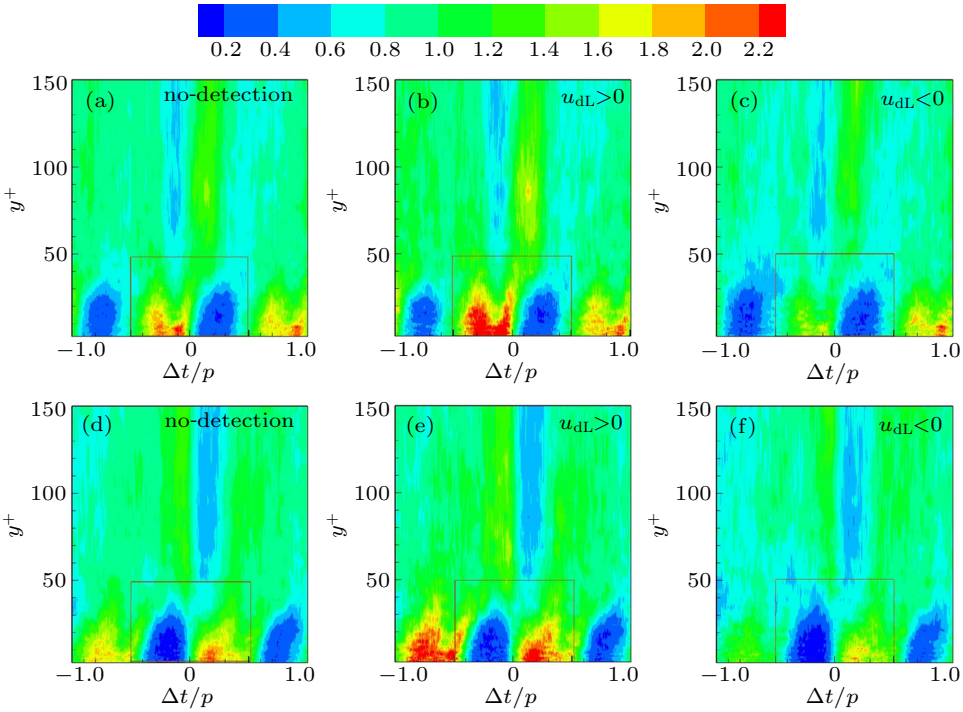


Fig. 10. Conditional average, $L\tilde{I}_{b,s}$, over zero-crossings of u_p: (a)–(c) positive to negative, (d)–(f) negative to positive in case A.

To investigate how the detecting signals interfer the controlling on small-scale local bursting intermittency, we need more evidence. Here, a parameter to characterize the local instantaneous intermittent events at the scale r based on $w_b(r,t)$ is defined as (similar with the local intermittency measure defined in expression (7))

$$LI_b(r,t) = \frac{w_b(r,t)^2}{\langle w_b(r,t)^2 \rangle}. \tag{9}$$

In the work by Tang *et al.*,[6] they conditioned LI_b on the zero-crossings of u_p to study the arrangement of the small-scale bursting intermittency and the perturbed fluctuations (u_p). Similarly, we condition LI_b on detecting signals u_{dL} and the zero-crossings of u_p, which is used to observe how the small-scale bursting events are arranged by both u_{dL} and u_p in the temporal domain. Specifically, we set the zero-crossings of u_p as the conditional location and study the small-scale bursting intermittency arrangements when the perturbed-scale fluctuations are changed from $u_P > 0$ to $u_P < 0$ (high to low speed) and from $u_P < 0$ to $u_P > 0$ (low to high speed) at $u_{dL} > 0$ or $u_{dL} < 0$. In this way, the small-scale bursting processes are phase averaged.

Figures 10–12 give the conditionally averaged results of the small-scale bursting events ($L\tilde{I}_{b,s}$) in controlled cases A, B, and C, respectively. For each controlled case, panels (a)–(c) represent the $L\tilde{I}_{b,s}$ (from $u_P > 0$ to $u_P < 0$) at no-detection, detecting signals $u_{dL} > 0$ and $u_{dL} < 0$. Panels (d)–(e) show the $L\tilde{I}_{b,s}$ (from $u_P < 0$ to $u_P > 0$) at no-detection, $u_{dL} > 0$ and $u_{dL} < 0$. As can be seen in all figures, there are apparently periodic low- and high-speed regions in $L\tilde{I}_{b,s}$ fields at the vibration frequency of $f_p = 160$ Hz in the near-wall region ($y^+ \leqslant 30$): a relatively low-intensity small-scale bursting process is observed in the low-speed region of perturbed mode ($u_P < 0$) and vice versa for the high-speed region. It means that the small-scale bursting intermittency is arranged by the perturbed-scale fluctuations. More interestingly, in each con-

trolled case, the detecting signals (u_{dL}) have an obvious modulation on the periodic regions in $L\tilde{I}_{\mathrm{b,s}}$ fields. As shown in Figs. 10(a)–10(f), compared with the no-detection case, the high-intensity regions in $L\tilde{I}_{\mathrm{b,s}}$ fields are apparently enhanced when $u_{\mathrm{dL}} > 0$, but weakened when $u_{\mathrm{dL}} < 0$. Meanwhile, the low-intensity regions in $L\tilde{I}_{\mathrm{b,s}}$ are almost unaffected by u_{dL}. This phenomenon also could be observed in Figs. 11 and 12. It has been proven above that the detecting signals obviously impact the small-scale bursting intensity: compared with the no-detecting case, increasing the intensity when $u_{\mathrm{dL}} > 0$ but weakening it when $u_{\mathrm{dL}} < 0$. Through Figs. 10–12, we could further indicate that this influence mainly focuses on the high-intensity regions of the small-scale bursting process rather than the low-intensity regions. Moreover, the high-intensity regions in $L\tilde{I}_{\mathrm{b,s}}$ are coupled with the high-speed regions of the perturbed signals ($u_{\mathrm{P}} > 0$), which reflects that the high-speed perturbed fluctuations might play a key role in the arrangement of detecting signals on the small-scale bursting process.

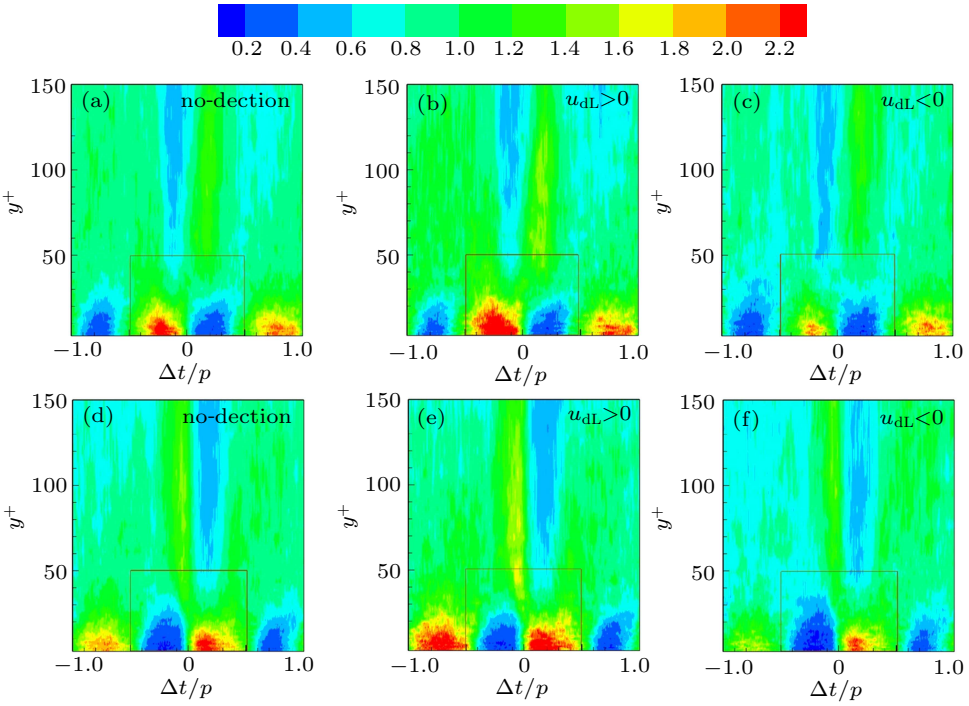


Fig. 11. Conditional average, $L\tilde{I}_{\mathrm{b,s}}$, over zero-crossings of u_{p}: (a)–(c) positive to negative, (d)–(f) negative to positive in case B.

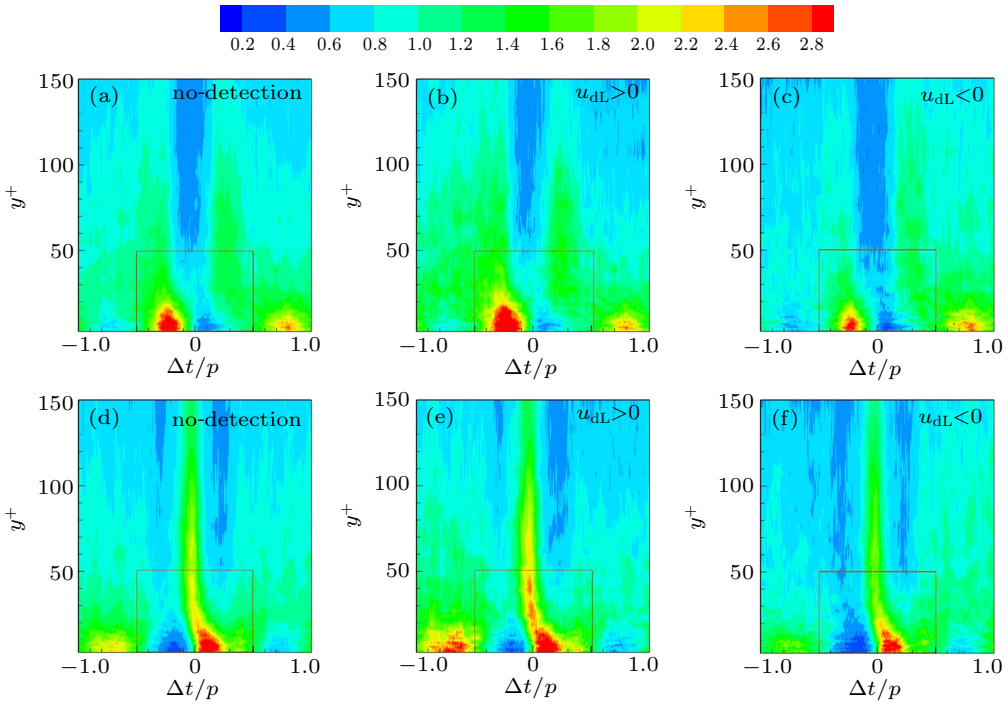


Fig. 12. Conditional average, $L\tilde{I}_{\mathrm{b,s}}$, over zero-crossings of u_{p}: (a)–(c) positive to negative, (d)–(f) negative to positive in case C.

4. Conclusions

Active control of a fully developed TBL over a flat plate has been studied. A single PZT actuator is employed to produce periodic input into the inner region of the TBL flow. A wall probe is fixed upstream of the actuator to identify the high- or low-speed large-scale fluctuations as the detecting signals. Then, the impact of the detecting signals on the small-scale bursting process is investigated based on the data acquired by the traversing probe downstream of the actuator. Furthermore, we also study how the detecting fluctuations interfere the arrangement of the perturbed mode on the small-scale bursting intensity. The major conclusions of the research are as follows.

(I) The actuator effectively disturbs the near-wall region of the TBL flow and reduces the drag. The drag reduction rate is positively related to the amplitude of the vibration. The maximum value of the rate is 18% in case A.

(II) The small-scale bursting process is obviously suppressed by the vibration in all controlled cases, and the detecting signals have an effect on this: compared with the no-detection case, the small-scale bursting intensity is restrained more apparently at high-speed detecting fluctuations but less impacted at low-speed detecting fluctuations.

(III) From a multi-scale perspective, the perturbed-scale fluctuations arrange the small-scale bursting process in the near-wall region. Moreover, the detecting signals have a clear impact on this arrangement, especially the high-intensity regions of the small-scale bursting events: the vibration enhances the intensity at high-speed detecting fluctuations but weakens it at low-speed detecting signals in these regions, which gives a direct evidence on how detecting signals interfering the small-scale bursting process.

References

[1] Blackwelder R F and Kaplan R E 1976 *J. Fluid Mech.* **76** 89
[2] Pan C and Wang J 2015 *Procedia IUTAM* **17** 101
[3] Corino E R and Brodkey R S 1969 *J. Fluid Mech.* **37** 1
[4] Adrian R J 2007 *Phys. Fluids* **19** 041301
[5] Blackwelder R F and Eckelmann H 1979 *J. Fluid Mech.* **94** 577
[6] Tang Z and Jiang N 2020 *Phys. Fluids* **32** 015110
[7] Jiménez J and Pinelli A 1999 *J. Fluid Mech.* **389** 335
[8] Schoppa W and Hussain F 2002 *J. Fluid Mech.* **453** 57
[9] Rebbeck H and Choi K S 1975 *Phys. Fluids* **18** 175
[10] Jiang D, Zhang H, Fan B, Zhao Z, Gui M and Chen Z 2019 *Ocean Eng.* **176** 74
[11] Ge M, Xu C and Cui G X 2015 *Acta Mech. Sin.* **31** 512
[12] Jiang D W, Zhang H, Fan B C and Wang A H 2019 *Chin. Phys. B* **28** 054701
[13] Tardu S 1995 *Exp. Fluids* **20** 112
[14] Tang, Zhanqi, Zheng, Xiaobo, Jiang, Nan, Wu and Yanhua 2016 *Experiments in Fluids* **57** 79
[15] Metzger M, McKeon B and ArceLarreta E 2010 *Physica D* **239** 1296
[16] Camussi R 1997 *J. Fluid Mech.* **348** 177
[17] Camussi R and Guj G 1999 *Phys. Fluids* **11** 423
[18] Antonia R A, Orlandi P and Romano G P 1998 *Phys. Fluids* **10** 3239
[19] Kim J, Moin P and Moser R 1987 *J. Fluid Mech.* **177** 133
[20] Onorato M, Camussi R and Iuso G 2000 *Phys. Rev. E* **61** 1447
[21] Cui X T, Jiang N, Zheng X B and Tang Z Q 2020 *Acta Mech. Sin.* **36** 12
[22] Xu C, Deng B, Huang W and Cui G 2013 *Sci. Chin.-Phys. Mech. & Astron.* **56** 1053
[23] Bai H L, Zhou Y, Zhang W G, Xu S J, Wang Y and Antonia R A 2014 *J. Fluid Mech.* **750** 316
[24] Zheng X B and Jiang N 2015 *Acta Mech. Sin.* **31** 16
[25] Smith C R and Metzler S P 1983 *J. Fluid Mech.* **129** 27
[26] Floryan J M and Saric W S 1983 *AIAA Journal* **21** 12
[27] Carlson H A and Lumley J L 1996 *J. Fluid Mech.* **329** 341
[28] She Z, Jackson E and Orszag S 1991 *Proc. R. Soc. A: Math. Phys. Eng. Sci.* **434** 101
[29] Zhang P, Liu A and Wang J 2010 *Sci. Chin. Technol. Sci.* **53** 2772
[30] Zheng X B, Jiang N and Zhang H 2016 *Chin. Phys. B* **25** 014703
[31] Zheng X B and Jiang N 2015 *Chin. Phys. B* **24** 064702
[32] Stefes B and Fernholz H H 2004 *Eur. J. Mech. B Fluids* **23** 303
[33] Patel V C and Head M R 1969 *J. Fluid Mech.* **38** 181
[34] Xin Y B, Xia K Q and Tong P 1996 *Phys. Rev. Lett.* **77** 1266
[35] Bai J X, Huang Y X, Jiang N, Ma X Y and Tang Z Q 2020 *Journal of Hydrodynamics* **32** 747
[36] Bai J X, Jiang N, Zheng X B, Tang Z Q, Wang K J and Cui X T 2018 *Chin. Phys. B* **27** 074701
[37] Farge M 1992 *Annual Review of Fluid Mechanics* **24** 395
[38] Daubechies I 1990 *Inf. Theory IEEE Trans.* **36** 961
[39] Kreplin H P and Eckelmann H 1979 *J. Fluid Mech.* **95** 305
[40] Johansson A V, Alfredsson P H and Kim J 1991 *J. Fluid Mech.* **224** 579
[41] Tang Z, Jiang N, Zheng X and Wu Y 2019 *Phys. Fluids* **31** 025120
[42] Meneveau and Charles 1991 *J. Fluid Mech.* **232** 469